Terahertz-Frequency Spin Hall Auto-oscillator Based on a Canted Antiferromagnet

O. R. Sulymenko,[1] O. V. Prokopenko,[1] V. S. Tiberkevich,[2] A. N. Slavin,[2] B. A. Ivanov,[1,3,4] and R. S. Khymyn[5]
[1]*Faculty of Radio Physics, Electronics and Computer Systems, Taras Shevchenko National University of Kyiv, Kyiv 01601, Ukraine*
[2]*Department of Physics, Oakland University, Rochester, Michigan 48309, USA*
[3]*Institute of Magnetism, National Academy of Science of Ukraine, Kyiv 03142, Ukraine*
[4]*Naional University of Science and Technology MISiS, Moscow 119049, Russian Federation*
[5]*Department of Physics, University of Gothenburg, 41296 Gothenburg, Sweden*
(Received 24 July 2017; revised manuscript received 16 October 2017; published 7 December 2017)

We propose a design of a terahertz-frequency signal generator based on a layered structure consisting of a current-driven platinum (Pt) layer and a layer of an antiferromagnet (AFM) with easy-plane anisotropy, where the magnetization vectors of the AFM sublattices are canted inside the easy plane by the Dzyaloshinskii-Moriya interaction (DMI). The dc electric current flowing in the Pt layer creates due to the spin Hall effect, a perpendicular spin current that, being injected in the AFM layer, tilts the DMI-canted AFM sublattices out of the easy plane, thus exposing them to the action of a strong internal exchange magnetic field of the AFM. The sublattice magnetizations, along with the small net magnetization vector $\mathbf{m}_{\mathrm{DMI}}$ of the canted AFM, start to rotate about the hard anisotropy axis of the AFM with the terahertz frequency proportional to the injected spin current and the AFM exchange field. The rotation of the small net magnetization $\mathbf{m}_{\mathrm{DMI}}$ results in the terahertz-frequency dipolar radiation that can be directly received by an adjacent (e.g., dielectric) resonator. We demonstrate theoretically that the radiation frequencies in the range $f = 0.05$–2 THz are possible at the experimentally reachable magnitudes of the driving current density, and we evaluate the power of the signal radiated into different types of resonators. This power increases with the increase of frequency f, and it can exceed 1 μW at $f \sim 0.5$ THz for a typical dielectric resonator of the electric permittivity $\varepsilon \sim 10$ and a quality factor $Q \sim 750$.

DOI: 10.1103/PhysRevApplied.8.064007

I. INTRODUCTION

One of the fundamental technical problems of the modern microwave and terahertz technology is the development of compact and reliable generators and receivers of coherent electromagnetic signals in the (0.1–10)-THz frequency range [1–3]. The terahertz frequency range has great potential for applications in medical imaging, security, material characterization, communications, control of technological processes, etc. There are several approaches to terahertz-frequency generation, including the use of free-electron lasers [4,5], quantum cascade lasers [6,7], superconductor Josephson junctions [8], backward-wave oscillators [5,9], electro-optic rectification of laser radiation [10], etc. However, all the abovementioned sources of terahertz-frequency signals require rather complex setups or low temperatures and/or cannot be made sufficiently small, which greatly limits their usability in many important practical applications.

Thus, there is a temptation to use alternative spin-dependent technologies to generate high-frequency electromagnetic signals. Indeed, the spintronic technology based on the dynamics of spin-polarized electric currents in thin multilayered ferromagnetic structures resulted in the development of spin-torque nano-oscillators (STNOs), which are manufactured using e-beam lithography and can be tuned by the variation of both the bias magnetic field and the bias direct current [11–17]. Unfortunately, the frequencies of the signals generated by STNOs are not very high and, typically, are limited to the interval of 1–50 GHz by the maximum bias magnetic field that can realistically be achieved in a portable spintronic device that uses ferromagnetic (FM) materials [18].

It was suggested some time ago [19–21] that one of the possible ways to substantially increase the frequency of the signals generated in magnetic layered structures is to use in them layers of an antiferromagnet (AFM) that possess a very strong internal magnetic field of the exchange origin which keeps the magnetization vectors of the AFM sublattices antiparallel to each other. Although this idea has been known for quite a while, a realistic theoretical proposal for the development of terahertz-frequency AFM-based spintronic nano-oscillators has been published only recently [21,22], soon after the first experimental observation of the switching of AFM sublattices under the action of a dc spin current [23,24].

In this work, we propose and theoretically analyze a terahertz-frequency signal generator based on the concept of a ferromagnetic spin-Hall oscillator (SHO) [11,15,25,26], but where the SHO free layer is made of a canted AFM (e.g., hematite α-Fe_2O_3) that has a small net

magnetization $\mathbf{m}_{\mathrm{DMI}}$ caused by the Dzyaloshinskii-Moriya interaction (DMI). We calculate the electromagnetic power emitted from the antiferromagnetic SHO due to the dipolar radiation from the rotating magnetization $\mathbf{m}_{\mathrm{DMI}}$ into the free space and into several types of transmission lines and resonators. Our analysis demonstrates that the output power P_{ac} of the AFM-based SHO increases with the generation frequency f, and it can exceed $P_{\mathrm{ac}} = 1\ \mu$W at $f \sim 0.5$ THz if a high-quality dielectric resonator is used to receive the generated signal.

II. MAGNETIZATION DYNAMICS INDUCED IN AFM BY AN EXTERNAL SPIN CURRENT

It was shown previously [19–21] that when a layer of an AFM is subjected to an external spin current, e.g., coming from an adjacent current-driven layer of a normal metal (NM) with strong spin-orbital interaction and polarized along a unit vector $\mathbf{p}$, a corresponding spin-transfer torque (STT) [27,28] is exerted on the sublattice magnetizations of the AFM. This STT can slightly tilt the AFM sublattice magnetizations $\mathbf{M}_1$ and $\mathbf{M}_2$, thus exposing them to the action of a large internal AFM magnetic field of the exchange origin, which starts to rotate the sublattice magnetizations about the vector $\mathbf{p}$ with a high angular frequency. For the experimentally achievable magnitudes of the spin current, the frequencies of this current-induced rotation lie the terahertz range. There is, however, a fundamental problem of how to extract the ac signal corresponding of that terahertz-frequency rotation from the spin-current-driven AFM, as this extraction is necessary to create a functioning source of a terahertz-frequency, AFM-based SHO.

This ac signal can be, in principle, picked up using the spin pumping produced by the rotating AFM magnetizations and inverse spin Hall effect (ISHE) in the adjacent NM layer. The ISHE voltage, however, is proportional to the instantaneous angular velocity of the AFM sublattice rotation, and, if the anisotropy of the chosen AFM material is *uniaxial* (i.e., isotropic in the magnetization rotation plane), the AFM rotation is, obviously, uniform in time, and the ISHE voltage is constant and does not contain any high-frequency ac components.

To extract a high-frequency ac signal from a current-driven AFM material containing rotating magnetic sublattices, two different approaches have been suggested. In the framework of a first approach, the feedback-induced nonlinear damping was used [21] for this purpose. However, there are serious practical problems with the use of the first approach, as it strongly relies on the quality of the NM-AFM interface and, also, requires rather high values of the spin-Hall angle in the NM. In the framework of the second approach, it was suggested to use a bianisotropic AFM, like nickel oxide (NiO), that has a relatively strong easy-plane anisotropy and a relatively weak easy-axis anisotropy in the perpendicular direction [22]. This additional anisotropy in the perpendicular direction creates an angular profile of the potential energy for the magnetic sublattices. An angular motion of the sublattice magnetizations $\mathbf{M_1}$ and $\mathbf{M_2}$ under the action of STT in this case is analogous to a viscous motion of a particle in a "washboard" potential under the action of a constant external force: the rotation of the magnetization vectors accelerates while moving towards the in-plane energy minima, and it decelerates while moving away from them. As a result, the rotational motion of the magnetizations is not uniform in time anymore, and, therefore, it can produce a high-frequency component in the voltage signal received in the NM layer through the ISHE. The ISHE voltage, which can be obtained by this mechanism, is proportional to the anisotropy in the perpendicular plane of the sublattice rotation [22], and one therefore needs a sufficiently high value of the anisotropy constant to produce a measurable resultant ac power. At the same time, the potential profile caused by the perpendicular anisotropy creates a barrier, which has to be overcome by the STT to start the sublattice rotation. That means that there will be a substantial threshold driving current, proportional to the in-plane anisotropy constant, needed to start the generation of the ac signal. In addition, it turns out that the ac signal created by the ISHE in a NM strongly decreases with the increase of the generation frequency, and it reaches a substantial power ($>1\ \mu$W) only in the range of relatively low frequencies, near the frequency of the in-plane antiferromagnetic resonance (approximately 100–300 GHz for a NiO SHO [22]).

Thus, it is necessary to find a way to extract ac signals from a current-driven AFM material that does not have a considerable perpendicular anisotropy and is practically uniaxial. One of the possible AFM materials of this kind is hematite (α-Fe_2O_3), in which the perpendicular anisotropy field is $H_e \simeq 0.2$ Oe, compared to $H_e \simeq 600$ Oe in the strongly bianisotropic NiO.

III. AFM CANTED BY THE DMI

In this work, we propose a qualitatively different approach to extract the generated ac signal from the AFM layer. We propose using in the layered structure of the SHO [22] a *canted* AFM (e.g., hematite) where magnetic sublattices are canted inside the easy plane by the DMI. This DMI-induced canting results in the formation of a small intrinsic net magnetization vector $\mathbf{m}_{\mathrm{DMI}}$ of the AFM. It can be shown that even the uniform rotation of the net magnetization vector $\mathbf{m}_{\mathrm{DMI}}$ with angular frequency $\omega = 2\pi f$ ($f = 0.05$–2 THz) leads to a substantial dipolar radiation of a high-frequency signal that can be received by different types of *external resonators*.

Therefore, we consider below a bilayered AFM-based SHO structure (see Fig. 1) consisting of a Pt layer and a hematite layer placed in an external resonator. For a quantitative estimation of parameters of the proposed

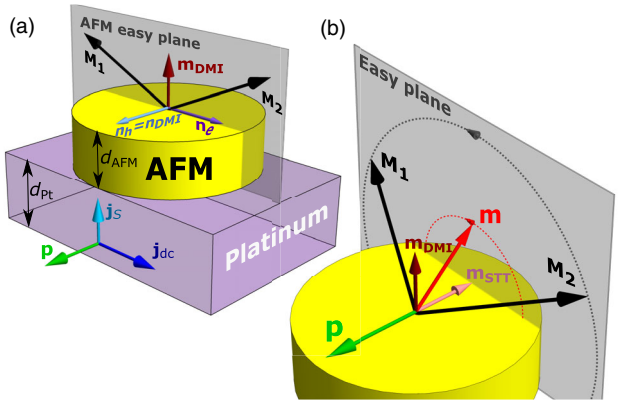

FIG. 1. (a) Schematics of an auto-oscillator based on a layered structure containing a Pt layer with a thickness d_{Pt} and an AFM layer with a thickness d_{AFM}. The AFM is shown in a ground state, where the sublattice magnetizations $\mathbf{M}_1$ and $\mathbf{M}_2$ lay in the easy plane of the AFM ($\mathbf{M}_1, \mathbf{M}_2 \perp \mathbf{n}_h$) and are canted by the DMI, thus producing a small net magnetization $\mathbf{m}_{\mathrm{DMI}}$. The direction of the STT polarization $\mathbf{p}$, required for the oscillations, is perpendicular to the easy plane ($\mathbf{p} \| \mathbf{n}_h$), which, in turn, defines the direction of the dc: $\mathbf{j}_{\mathrm{dc}} \perp \mathbf{n}_h$. (b) The STT with polarization $\mathbf{p}$ creates a magnetic moment $\mathbf{m}_{\mathrm{STT}} \| \mathbf{p}$. The sublattices $\mathbf{M}_1$ and $\mathbf{M}_2$, as well as the net magnetic moment $\mathbf{m} = \mathbf{m}_{\mathrm{STT}} + \mathbf{m}_{\mathrm{DMI}}$, start to rotate on a cone with a base in the AFM easy plane. The rotation trajectories are indicated by dotted arcs.

AFM-based SHO, we use the following typical parameters of the layered structure: it is a circular disk with a radius $r_{\mathrm{SHO}} = 10\ \mu$m and a thickness d_{AFM} of 5 nm made of hematite and covered by a 20-nm-thick platinum layer (see Fig. 1).

The bulk DMI inside the AFM layer leads to the canting of the magnetizations $\mathbf{M}_1$ and $\mathbf{M}_2$ of the AFM sublattices, thus creating a small net magnetization $\mathbf{m}_{\mathrm{DMI}} = \mathbf{M}_1 + \mathbf{M}_2$. The spin dynamics of an AFM with biaxial anisotropy under the influence of a STT created by an external spin current is described by two coupled Landau-Lifshitz equations for the vectors $\mathbf{M}_1$ and $\mathbf{M}_2$:

$$\frac{d\mathbf{M}_i}{dt} = \gamma\mu_0[\mathbf{H}_i \times \mathbf{M}_i] + \frac{\alpha_{\mathrm{eff}}}{M_s}\left[\mathbf{M}_i \times \frac{d\mathbf{M}_i}{dt}\right] + \frac{\tau}{M_s}[\mathbf{M}_i \times [\mathbf{M}_i \times \mathbf{p}]], \quad (1)$$

where $i = 1, 2$ are the indices denoting the AFM sublattices, γ is the modulus of the gyromagnetic ratio, μ_0 is the vacuum permeability, M_s is the magnitude of saturation magnetization of the AFM sublattices, α_{eff} is the effective AFM Gilbert damping parameter, τ is the amplitude of the STT caused by the spin current transferred from the current-driven Pt layer into the AFM layer, $\mathbf{p}$ is a unit vector along the spin-current polarization, and $\mathbf{H}_i$ is the effective magnetic field acting on the sublattice $\mathbf{M}_i$:

$$\mathbf{H}_{1,2} = [-H_{\mathrm{ex}}\mathbf{M}_{2,1} - H_h\mathbf{n}_h(\mathbf{n}_h \cdot \mathbf{M}_{1,2}) + H_e\mathbf{n}_e(\mathbf{n}_e \cdot \mathbf{M}_{1,2}) \mp H_{\mathrm{DMI}}[\mathbf{n}_{\mathrm{DMI}} \times \mathbf{M}_{2,1}]]/M_s. \quad (2)$$

Here, H_{ex} is the exchange field, H_e and H_h are the in-plane and perpendicular-to-plane anisotropy fields, respectively, $\mathbf{n}_e$ and $\mathbf{n}_h$ are the unit vectors along the "easy" and "hard" anisotropy axes, H_{DMI} is the effective field caused by the DMI, and $\mathbf{n}_{\mathrm{DMI}}$ is the DMI vector.

The STT amplitude expressed in the frequency units [22,29] is

$$\tau = j_{\mathrm{dc}} g_{\uparrow\downarrow} \theta_{\mathrm{SH}} \frac{e\gamma\lambda_{\mathrm{Pt}}\rho_{\mathrm{Pt}}}{2\pi M_s d_{\mathrm{AFM}}} \tanh\frac{d_{\mathrm{Pt}}}{2\lambda_{\mathrm{Pt}}}, \quad (3)$$

where j_{dc} is the density of the dc electric current in the platinum layer, $g_{\uparrow\downarrow}$ is the spin-mixing conductance at the Pt-AFM interface, θ_{SH} is the spin-Hall angle in Pt, e is the modulus of the electron charge, λ_{Pt} is the spin-diffusion length in the Pt layer, ρ_{Pt} is the electric resistivity of Pt, and d_{AFM} and d_{Pt} are the thicknesses of the AFM and Pt layers, respectively.

The effective damping parameter α_{eff} of the layered structure in Eq. (1) includes the additional magnetic losses due to the spin pumping from the AFM layer into the adjacent Pt layer:

$$\alpha_{\mathrm{eff}} = \alpha_0 + \alpha_{\mathrm{SP}} = \alpha_0 + g_{\uparrow\downarrow}\frac{\gamma\hbar}{4\pi M_s d_{\mathrm{AFM}}}, \quad (4)$$

where α_0 is the intrinsic Gilbert damping constant and $\hbar$ is the reduced Planck constant.

As was shown in Ref. [22], the presence of the anisotropy H_e in the plane perpendicular to the spin-polarization direction $\mathbf{p}$ makes the current-driven magnetization dynamics in AFM nonuniform in time and also determines the threshold charge current at which the auto-oscillatory dynamics starts. Thus, to minimize the threshold of auto-oscillations, one should choose an almost purely "easy-plane" AFM with $\mathbf{n}_h \| \mathbf{p}$ and a low value of the perpendicular anisotropy ($H_e \ll H_h$). The DMI vector $\mathbf{n}_{\mathrm{DMI}}$ is commonly directed along one of the AFM crystallographic axes. If $\mathbf{n}_{\mathrm{DMI}} \| \mathbf{n}_h$, the DMI creates a small net magnetization which lies in the easy plane of the AFM, $\mathbf{m}_{\mathrm{DMI}} \perp \mathbf{n}_h$. The above-described geometrical relations are realized, for example, in α-Fe_2O_3 (hematite) and $FeBO_3$.

Below, we consider in detail the SHO based on a thin film of hematite, which has almost purely easy-plane anisotropy ($H_e = 0.2$ Oe $= 15.9$ A/m, while $H_h = 200$ Oe $= 15.9 \times 10^3$ A/m and $H_{\mathrm{ex}} = 9 \times 10^6$ Oe $= 0.7 \times 10^9$ A/m) and net magnetization moment $m_{\mathrm{DMI}} = M_s H_{\mathrm{DMI}}/H_{\mathrm{ex}} = 2100$ A/m caused by the $H_{\mathrm{DMI}} = 22 \times 10^3$ Oe $= 1.75 \times 10^6$ A/m [30–33]. The intrinsic magnetic damping of hematite is rather low, $\alpha_0 \simeq 10^{-4}$, while the effective

damping that takes into account the spin pumping into the adjacent Pt layer [see Eq. (4)] is $\alpha_{\text{eff}} = 2 \times 10^{-3}$.

We solve Eq. (1) numerically for the case where the spin-current polarization $\mathbf{p} \| \mathbf{n}_h$, with the main material and geometric parameters taken from Ref. [22]. In this case, the STT [i.e., the last term in Eq. (1)] tilts the AFM sublattice magnetizations $\mathbf{M}_1$ and $\mathbf{M}_2$ out of the easy plane of the AFM and creates the net magnetic moment

$$m_{\text{STT}} = \frac{\tau M_s}{\alpha_{\text{eff}} \gamma H_{\text{ex}}} \tag{5}$$

in the out-of-plane direction $\mathbf{m}_{\text{STT}} \| \mathbf{p} \| \mathbf{n}_h$. Now, the total net magnetization reads as $\mathbf{m} = \mathbf{m}_{\text{DMI}} + \mathbf{m}_{\text{STT}}$ [see Fig. 1(b)] and $\mathbf{m}_{\text{DMI}} \perp \mathbf{m}_{\text{STT}}$.

The $\mathbf{M}_1$ and $\mathbf{M}_2$ magnetizations and, consequently, $\mathbf{m}_{\text{DMI}}$, which are now exposed to the action of the internal exchange field, start to rotate around $\mathbf{p}$ with the angular velocity $\omega = 2\pi f = \tau/\alpha_{\text{eff}}$. This rotation is almost uniform in time due to the low value of the in-plane anisotropy in hematite.

The rotation frequency f and the net magnetization m_{STT} are shown as functions of the electric current density flowing in the Pt layer in Fig. 2. To obtain these curves, it is necessary to know the value of the spin-mixing conductance $g_{\uparrow\downarrow}$ at the Pt-hematite interface. Although there exist several studies of the electronic structure of hematite [34–36], we have not found a reliable value of $g_{\uparrow\downarrow}$ in literature. For numerical simulations, we choose a value $g_{\uparrow\downarrow} = 6.9 \times 10^{14}$ cm^{-2}, which was previously obtained for the Pt-NiO interface [37] and is in a good agreement with the rough estimations made by the method developed in Ref. [38]. The assumption for the $g_{\uparrow\downarrow}$ magnitude also allows us to make a direct comparison of both the general

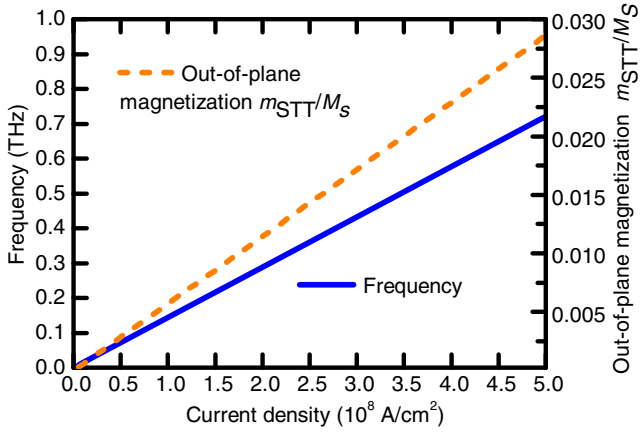

FIG. 2. Calculated frequency of the generated ac signal f (the solid line, left axis) and normalized magnitude of the out-of-plane magnetization m_{STT}/M_s (the dashed line, right axis) in a SHO based on a canted AFM (hematite) as functions of the dc driving current density j_{dc} in the adjacent Pt layer for the hematite film thickness of $d_{\text{AFM}} = 5$ nm.

properties and the intrinsic spin dynamics for the SHO based on hematite and a similar auto-oscillator based on the NiO one [22].

As one can see in Fig. 2, the generation frequency f can be controlled by the density j_{dc} of the electric current injected into the Pt layer. For instance, the current density j_{dc} that is required to get the generation at the frequency of $f = 0.5$ THz is $j_{\text{dc}} = 3.5 \times 10^8$ A/cm^2, which was previously achieved in an experiment [15].

IV. DIPOLAR ELECTROMAGNETIC RADIATION OF A ROTATING NET MAGNETIZATION IN A CANTED AFM

To investigate the possibility of power extraction from a SHO based on a Pt/AFM layered structure, let us first consider the electric current in a Pt layer produced by the ISHE caused by a current-driven rotation of the AFM sublattice magnetizations. The density of the spin current flowing back from the AFM layer to the adjacent Pt layer $\mathbf{j}_s^{\text{out}}$ can be written as

$$\mathbf{j}_s^{\text{out}} = \frac{\hbar g_{\uparrow\downarrow}}{4\pi M_s^2} \sum_{i=1,2} (\mathbf{M}_i \times \dot{\mathbf{M}}_i). \tag{6}$$

In our case involving easy-plane AFM with DMI, the total net magnetization caused by the DMI is precessing along a cone of the height m_{STT} and cone base radius m_{DMI} (see Fig. 1). Therefore, the ac component of the current $\mathbf{j}_s^{\text{out}}$ [see Eq. (6)] is proportional to the product of *two small quantities*—$m_{\text{DMI}} m_{\text{STT}}$ and, consequently, in the considered frequency range it is negligibly small (see Fig. 2). Specifically, we obtain a maximum output power of less than 100 pW at $f = 1$ THz for a square hematite sample having a 200-μm^2 surface area. Such a low value of the output power makes the ISHE practically useless as a method of the signal extraction in the frequency range $2\pi f \ll \gamma \mu_0 H_{\text{ex}}$, and it is necessary to find other ways to extract an output ac signal from a SHO based on a canted AFM with negligible in-plane anisotropy.

Fortunately, in a canted AFM crystal, having a small net magnetization, the current-induced precession of this magnetization can be detected not only through the ISHE but also *directly* through the dipolar radiation produced by this precessing magnetization. The rotating magnetization of the AFM-based SHO $\mathbf{m}_{\text{DMI}}$ creates an oscillating dipolar magnetic field that can be received, channeled, and then utilized if the generating SHO is coupled to an appropriate resonator.

The problem involving direct dipolar emission of an ac signal generated by a precessing magnetization was considered in Ref. [39] for the case of a conventional microwave-frequency STNO. It was shown in Ref. [39] that the dipolar emission mechanism might become preferable

TABLE I. Expressions for $V_{\rm eff}$ and values for the ac power emitted by a SHO at $f = 0.5$ THz calculated using Eq. (7).

Case	Expression for $V_{\rm eff}$	Parameters	Maximum power, W
Free space	$3c^3/8\pi^3 f^3$	$f = 0.5$ THz, $c = 3\times10^8$ m/s, $Q = 1$	2.6×10^{-12}
Nanoloop	$r_{\rm SHO}^2 R_L/2\mu_0\pi^2 f$	$R_L = 6030\ \Omega$, $Q = 1$	1.4×10^{-10}
Rectangular waveguide	$2a^2b\chi/\pi^2$	$a = 0.47$ mm, $b = 50$ nm, $\chi = \eta/\sqrt{1-\eta^2}$, $\eta = c/2af \approx 0.64$, $Q = 1$	2.3×10^{-8}
Dielectric waveguide	$2a^2b\chi_\varepsilon/\pi^2$	$a = 0.47$ mm, $b = 50$ nm, $\chi_\varepsilon = \eta_\varepsilon/\sqrt{1-\eta_\varepsilon^2}$, $\eta_\varepsilon = c/2af\sqrt{\varepsilon} \approx 0.2$, $\varepsilon = 10$, $Q = 1$	2.9×10^{-8}
Parallel-plate line	$8abc/\pi^2 f$	$a = 0.47$ mm, $b = 50$ nm, $Q = 1$	1.2×10^{-9}
Rectangular resonator	$8a^4b\chi^3f^2/c^2$	$a = 0.47$ mm, $b = 50$ nm, $Q = 10$	2.26×10^{-9}
Parallel-plate resonator	$2abc/f$	$a = 0.47$ mm, $b = 50$ nm, $Q = 2$	9.7×10^{-10}
Dielectric resonator	$2a^2b\chi_\varepsilon$	$a = 0.47$ mm, $b = 50$ nm, $\varepsilon = 10$, $Q = 750$	1.1×10^{-6}

for a case of magnetic devices operating at frequencies above 0.1 THz, which makes this mechanism promising for application in the terahertz-frequency AFM-based SHOs.

To calculate the ac power $P_{\rm ac}$ that can be emitted by the SHO into a free space, different transmission lines (rectangular waveguide, parallel-plate waveguide, dielectric waveguide) and different resonators (rectangular, parallel plate, dielectric) we use the simple model of a direct dipolar emission from a system of two effective magnetic dipoles developed in Refs. [39,40]. In the framework of this approach, we use the expressions for the fields of a magnetic dipole obtained in Refs. [40,41] and the standard expressions for the electromagnetic fields of fundamental modes in the considered transmission lines and resonators presented in Ref. [41]. Also, to simplify the theoretical analysis of the electromagnetic-field excitation in a rectangular dielectric waveguide and resonator by a net ac magnetization $\mathbf{m}_{\rm DMI}$, we use the approximate magnetic-wall boundary conditions [41]. Unfortunately, the exact analytical solution for this problem has not yet been found.

In our approximate calculation, we assume that the rotating net magnetization of the AFM-based SHO $\mathbf{m}_{\rm DMI}$ is spatially uniform (macrospin approximation), and that the sizes of the effective magnetic dipoles (defined by the in-plane dimensions of the SHO) are substantially smaller than the wavelength λ of the ac signal. To evaluate the maximum magnitude of the emitted ac power, we take the magnitude of the ac magnetization $\mathbf{m}_{\rm DMI}$ from the numerical solution of Eq. (1).

Using the above-described model, we perform full electrodynamic calculations of the power emitted by an AFM-based SHO into different microwave- and terahertz-frequency resonators and transmission lines (see the Appendix for details), and we find that, in all cases, the maximum emitted ac power can be expressed by the following generalized expression:

$$P_{\rm ac} = P_m \frac{V}{V_{\rm eff}} Q. \tag{7}$$

Here, $P_m = \mu_0 m_{\rm DMI}^2 V f$ is the characteristic ac power generated in the SHO by the rotating magnetization $\mathbf{m}_{\rm DMI}$, f is the frequency of the generated ac signal, $V = \pi r_{\rm SHO}^2 d_{\rm AFM}$ is the volume of the AFM layer, Q is the quality factor of a particular resonance system, and $V_{\rm eff}$ is the frequency-dependent effective volume of a particular resonance system coupled to the AFM-based SHO. Basically, the expressions for $V_{\rm eff}$ obtained for the electromagnetic-energy emission into free space (far-field zone)—a nanoloop (near-field zone), rectangular and dielectric waveguides, a parallel-plate line, and rectangular, parallel-plate, and dielectric resonators—represent the results of electrodynamic calculation, and they can be used to compare the efficiency of AFM-based signal generators coupled to different resonance systems (see Table I).

It follows from Eq. (7) that a significant output ac power $P_{\rm ac}$ can be obtained only when the resonator coupled to the AFM-based SHO has a reasonably high quality factor ($Q \gg 1$), and the SHO is operating at a sufficiently high frequency, as P_m *increases* with the increase of the generation frequency f. This generation frequency can be controlled by the magnitude of the driving current density (see Fig. 2). It is also important to have a sufficiently small "effective volume" $V_{\rm eff}$ of the SHO resonator, which, in the ideal case, should be comparable to the volume V of the AFM layer.

The extracted ac power should be substantially smaller in the case of radiation into a transmission line where $Q = 1$ and/or the effective volume $V_{\rm eff}$ is, typically, substantially larger than the volume of the AFM layer.

To decrease the effective volume of the resonance system, one can fill it with a dielectric having a large dielectric permittivity ε. This approach is well known in the field of microwave- and terahertz-frequency technology [41]. A simple qualitative analysis shows that a high-Q terahertz-frequency dielectric resonator can be an effective system for the extraction of the generated ac power from an AFM-based SHO. It is also obvious that the intrinsic ac power $P_m \sim fV$ and the efficiency of the ac power

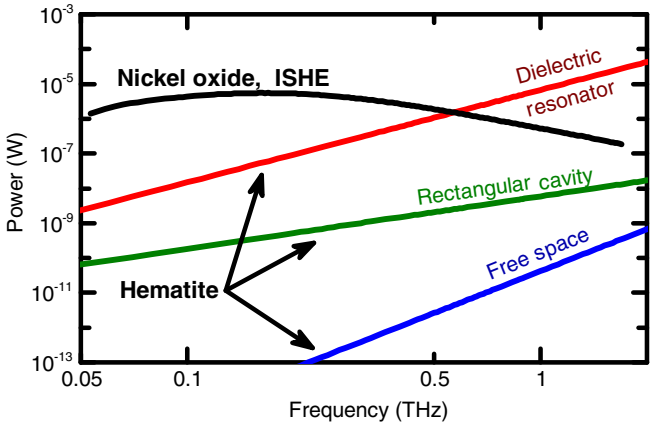

FIG. 3. Generated power vs frequency for a SHO based on a layer (thickness, $d_{\mathrm{AFM}} = 5$ nm) of a canted AFM providing dipolar radiation into different types of resonance systems: dielectric resonator (the red line), rectangular cavity (the green line), and free space (the blue line). For comparison, a similar curve is presented for a SHO based on a layer of bianisotropic AFM (NiO) where the generated ac signal is extracted through the ISHE in the adjacent Pt layer (the black line demonstrating a decrease of the generated power with frequency).

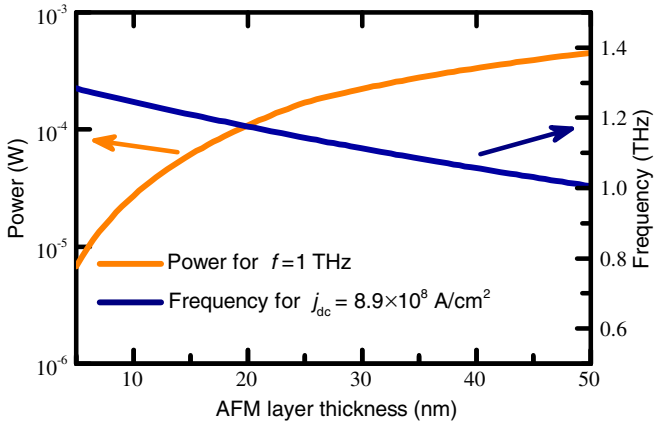

FIG. 4. Power and frequency of a signal generated in a SHO based on a canted AFM (hematite) as functions of the AFM layer thickness. The power was calculated for the generated frequency $f = 1$ THz, while the frequency is calculated at the driving dc current $j_{\mathrm{dc}} = 8.9 \times 10^8$ A/cm^2.

extraction using the dipolar radiation mechanism are higher for the AFM-based SHOs than for the conventional ferromagnetic STNO. The reasons for that are, first of all, the much higher frequencies f generated by AFM-based SHOs ($f \sim 1$ THz in a SHO, while it is $f \sim 10$ GHz in a typical STNO; see Fig. 2), and a substantially larger active magnetic layer volume V in an AFM-based SHO than found in a STNO (typical radius of a conventional circular STNO is about 100 nm, while the radius of an antiferromagnetic SHO can be 100 or more times larger).

Despite a relatively small magnitude of the net magnetization $\mathbf{m}_{\mathrm{DMI}}$ rotating inside a canted AFM and, consequently, a relatively small magnitude of the intrinsic power P_m, one can obtain a substantial output power P_{ac} of the total autogenerator based on a layer of a canted AFM in the case of a sufficiently high generation frequency f.

Using Eq. (7), we calculate the maximum ac power P_{ac} radiated by a hematite-based SHO into different resonance structures (free space, rectangular and dielectric resonator) as functions of the generated frequency. These curves are shown in Fig. 3. In Fig. 3, the blue line shows the dependence $P_{\mathrm{ac}}(f)$ for a hematite SHO ($d_{\mathrm{AFM}} = 5$ nm) radiating into free space, while the green and red lines show the dependence $P_{\mathrm{ac}}(f)$ for the hematite-based SHO coupled to a rectangular cavity and a high-Q dielectric resonator, respectively. For comparison, a similar curve (the black line) is presented for a SHO based on a layer of a bianisotropic AFM (NiO) ($d_{\mathrm{AFM}} = 5$ nm), where the generated ac signal is extracted through the ISHE in the adjacent Pt layer. It is clear that the signal-extraction method based on the ISHE has an advantage at relatively low frequencies, but the method based on the dipolar radiation from a canted AFM wins in the limit of high terahertz frequencies.

The dependencies of the power and frequency of a signal generated in a SHO based on a canted AFM (hematite) on the AFM layer thickness are presented in Fig. 4. The power is calculated for the generated frequency $f = 1$ THz, while the frequency is calculated at the driving dc current $j_{\mathrm{dc}} = 8.9 \times 10^8$ A/cm^2. As mentioned above, the generation frequency f depends on the ratio of the STT τ to the effective damping constant α_{eff} as $2\pi f = \tau/\alpha_{\mathrm{eff}}$. The damping constant α_{eff} [see Eq. (4)] includes the contribution of the intrinsic AFM damping α_0, which we assume does not depend on the AFM thickness, and the loss of the spin angular momentum due to the spin pumping, α_{SP}. Since the STT and the spin pumping share the same origin and are, for practical purposes, the interfacial effects because of the small spin-diffusion length in the AFM insulators, both the STT τ and the spin-pumping-induced damping α_{SP} are inversely proportional to the AFM thickness d_{AFM} [see Eqs. (3) and (4)]. Therefore, in the limiting case where $\alpha_0 = 0$, the generation frequency does not depend on the AFM thickness at all. For most AFM insulators, α_0 is relatively small and, for sufficiently thin AFM films, the ratio $\alpha_0 \ll \alpha_{\mathrm{SP}}$ holds. In this case, as one can see in Fig. 4, the increase of the AFM layer thickness leads to a moderate decrease of the generated frequency, but, at the same time, to a substantial increase of the generated power—which, in turn, is proportional to d_{AFM}. Obviously, in the opposite case, when $\alpha_{\mathrm{SP}} \ll \alpha_0$, which is realized for a thick AFM layer ($d_{\mathrm{AFM}} > 100$ nm for hematite), the frequency of the oscillations decreases as $1/d_{\mathrm{AFM}}$. Interestingly, the last case is common for STT oscillators based on FM metals, even those having rather thin FM layers, due to the large Gilbert damping constant

$\alpha_0 \simeq 0.01$ in the FM metals. It should also be noted that the calculation results presented in Fig. 4 are obtained in the macrospin approximation, which is quantitatively correct only for sufficiently thin AFM layers (probably thinner than 20–30 nm). However, the relatively weak dependence of the generation frequency and a substantially stronger dependence of the generated power on the thickness of the AFM layer is practically important, and a more accurate micromagnetic calculation should be used in the future to optimize the AFM thickness in the practical AFM-based signal generators.

The general expressions for the effective volume V_{eff}, along with the system's parameters and the values of P_{ac} (calculated at a generation frequency of $f = 0.5$ THz), are presented in Table I (see the Appendix for details).

The results presented in Table I and Fig. 3 (the blue line) demonstrate that the power emitted from an AFM-based SHO operating at a frequency $f = 0.5$ THz into free space is very low. If we place a SHO in the center of a gold-wire nanoloop of a round shape (with a radius $r_L = 100$ μm, a square cross section of the wire $S_L = 50 \times 50$ nm^2, and a characteristic resistance $R_L = 2\pi\rho_{\text{Au}} r_L / S_L = 6030$ Ω, where $\rho_{\text{Au}} = 24$ nΩ m is the resistivity of gold), we can increase the emitted power by approximately 10^2 times because the power can be collected by the loop in a near-field zone (see Table I) [39].

To increase the generated power, we can also place an AFM-based SHO in a waveguide (rectangular, parallel plate, or dielectric). In this case, the electromagnetic field generated by a SHO can excite fundamental propagating modes in these transmission lines, but, as can be seen in Table I, this approach is not very effective because, for the considered waveguides, $Q = 1$ and $V_{\text{eff}} \gg V$, which, in accordance with Eq. (7), leads to rather small values of P_{ac}.

In order to substantially enhance the emitted power, a SHO should be placed in a microwave- or terahertz-frequency resonator with a sufficiently high Q factor, which allows one to increase the emitted power Q times [see Eq. (7)]. Our calculations performed for rectangular, parallel-plate, and dielectric resonators having sizes $a \times b \times l$ and reasonably high frequency-dependent quality factors $Q \equiv Q(f)$ [42] demonstrate that the power emitted into rectangular or parallel-plate resonators having metal walls is comparable to the power that can be extracted from a SHO placed in a transmission line, mainly due to the increase of the Ohmic losses in the resonator walls (both resonators) and radiation losses (a parallel-plate resonator).

The power emitted into a resonator can be increased if the effective volume V_{eff} of the resonator is reduced, while its quality factor remains sufficiently large. To achieve this effect, it is possible to, e.g., place a SHO inside a dielectric resonator having a resonance frequency $f = 0.5$ THz (mode TM_{101}), reasonable size ($470\,\mu\text{m} \times 50\,\text{nm} \times 97\,\mu\text{m}$), the dielectric permittivity $\varepsilon = 10$, and the Q factor $Q = 750$. In such a case, the power emitted by the AFM-based SHO into a dielectric resonator can reach $P_{\text{ac}} = 1.1$ μW (see Table I and the red line in Fig. 3). It is clear from Fig. 3 and Table I that the design of an AFM-based SHO involving a high-Q dielectric resonator could be promising for the development of practical terahertz-frequency ac signal sources based on the antiferromagnetic SHOs.

At the same time, at frequencies higher than 1 THz, the use of quasioptical resonators might turn out to be preferable. Also, as is clear from Fig. 4, an additional enhancement of the ac power P_{ac} emitted from an AFM-based SHO can be achieved by increasing the thickness d_{AFM} of the AFM layer. This change will lead to an increase of the AFM layer volume $V \sim d_{\text{AFM}}$ and, therefore, to an increase in the power of the magnetization oscillations P_m [see Eq. (7)].

Finally, it is interesting, for comparison, to consider a bianisotropic AFM crystal with no DMI (e.g., NiO) where the ac component of the output spin current can reach a substantial magnitude if the AFM sublattice rotation is nonuniform in time [22]. In this case, the ac component of the current $\mathbf{j}_s^{\text{out}}$ is proportional to the acceleration in the rotation of the sublattice magnetizations. The SHO based on this effect was proposed in Ref. [22], where the small in-plane anisotropy of NiO makes the sublattice rotation nonuniform in time. The calculated output power of such a NiO SHO is shown in Fig. 3 by a black solid line. To make a direct comparison with the case of an easy-plane hematite SHO, we assume that both types of AFM-based SHOs have the same surface area. As one can see in Fig. 3, the output power of the NiO SHO decreases with the increase of the generation frequency, and this device and this method of ac signal extraction become noncompetitive for generation frequencies above 0.5 THz.

To understand what the area of possible practical applications of the proposed terahertz-frequency generators based on the AFM SHO is, it is very useful to compare their characteristics (frequency range, ac power, specific features, and experimental requirements) with the characteristics of existing terahertz-frequency generators and gigahertz-frequency generators based on FM materials. The results of this comparison are summarized in Table II. As one can see, in contrast to many of the considered generator systems, the proposed AFM-based generators integrated with high-Q dielectric resonators do not require complex setups, can be easily fabricated, and have sizes less than 1 mm. Although the operation frequency of these generators is limited by the AFM resonance frequency f_{AFMR} and, for typical materials, is below 1 THz [25], the ac power extracted from such a device can substantially exceed 1 μW, which is a characteristic maximum value of the ac power that can be obtained from FM-based STNOs at frequencies of

TABLE II. Comparison of the proposed terahertz-frequency AFM-based SHO with existing terahertz- and gigahertz-frequency generators.

Type of generator	Typical frequency range	Typical ac power	Comments	References
Proposed AFM-based SHO	0.1–10 THz	0.1–500 μW	P_{ac} increases with frequency f	...
Other AFM-based SHOs	0.1–1.5 THz	$0.1-1\mu$W	P_{ac} reaches maximum at frequencies $f \sim 0.1$ THz	[21,22]
Gyrotron	0.1–0.5 THz	1 kW–5 MW	Large complex setup, high voltage, strong dc magnetic field are required	[5]
Backward-wave oscillator	0.03–1.5 THz	1 mW–1 W	Sizes $\gtrsim$1 cm, high voltage is required	[5,9]
Free-electron laser	1–4 THz	1 W–10 kW (peak power)	Large complex setup, high voltage, strong dc magnetic field are required	[4,5,10]
Quantum cascade laser	0.5–3 THz	0.1–1 μW	Complex setup, works at low temperatures ($\lesssim$100 K)	[6,7]
Semiconductor-heterostructure laser	4.4 THz	$\gtrapprox 2$ μW	Complex setup, works at low temperatures ($\lesssim$10 K)	[43]
Electro-optic rectification of laser radiation	0.1–1 THz	1 μW – 1 mW	An external terahertz-frequency pumping source is required	[10]
Unitraveling-carrier photodiode	0.1–1 THz	10 μW–10 mW	ac power greatly reduces with an increase of frequency f	[10]
Josephson oscillator	0.1–1 THz	1 nW–1 μW	Complex setup, works at cryogenic temperatures	[8]
FM-based SHO	$10^{-3}-10^{-2}$ THz	1–10 pW	ac power has been too low thus far	[11,15,25,26,44]
FM-based STNO	10^{-3}–5×10^{-2} THz	100 pW–1 μW	ac power typically reduces with an increase of frequency f	[11–18]

about 1 GHz. Also, the frequency and power values of the above-considered AFM-based SHO greatly exceed the corresponding characteristics of the FM-based SHOs. The above-proposed oscillator based on the canted AFM materials has substantial advantages over other AFM-based SHOs that were recently investigated in Refs. [21,22]. In contrast to the previously considered AFM-based SHOs [21,22], where the SHO's output power is reduced at frequencies $f > f_{AFMR}$, our SHO has an important advantage—its output power increases with an increase of the generation frequency f, which makes this generator promising for applications at the high end of the terahertz frequency range. We believe that the abovementioned interesting and useful properties of the proposed terahertz-frequency AFM-based generator could be employed in the development of low- and medium-power sources of terahertz-frequency signals for practical applications in terahertz spectroscopy, medical imaging, etc.

V. CONCLUSIONS

In this work, we demonstrate theoretically that a SHO based on a canted antiferromagnet (e.g., hematite) can be used for the development of terahertz-frequency ac signal sources, where the power of a generated ac signal can be extracted from a SHO through the dipolar oscillating magnetic field created by the current-driven rotating net magnetization of the canted AFM. We show that the efficiency of this mechanism of the ac power extraction increases with an increase of signal frequency, and that it depends on the Q factor and the effective volume of the attached microwave- or terahertz-frequency resonance system. Our analysis also shows that the output ac power of such a terahertz-frequency signal source could exceed 1 μW at the frequency $f \sim 0.5$ THz for the hematite or Pt SHO coupled to a dielectric resonator with reasonable experimental parameters (size 470 μm $\times$ 50 nm $\times$ 97 μm, dielectric permittivity $\varepsilon = 10$, and Q factor $Q = 750$). The above-proposed SHO based on a current-driven layered structure of a canted AFM and Pt and incorporating an external dielectric resonator has a practically interesting level of the output power, and its efficiency increases with the increase of the generation frequency, in contrast to the NiO SHO proposed in Ref. [22], which relies on the ISHE mechanism for the extraction of the ac power. The obtained results could become critically important for the development and optimization of practical terahertz-frequency nano- and microscale electromagnetic signal sources.

ACKNOWLEDGMENTS

This work was supported financially by Grants No. EFMA-1641989 and No. ECCS-1708982 from the NSF, by the Knut and Alice Wallenberg Foundation (KAW), by the Center for NanoFerroic Devices (CNFD) and the Nanoelectronics Research Initiative (NRI), by DARPA M3IC grant, by the Taras Shevchenko National University of Kyiv, Ukraine (Grant No. 16BF052-01), by the National Academy of Sciences of Ukraine via Grant No. 7F and Project No. 1/17-N, by the Ministry of

Education and Science of the Russian Federation in the framework of the Increase Competitiveness Program of NUST MISiS (Grant No. K2-2017-005), implemented by a governmental decree dated March 16, 2013 (N 211). The publication also contains results of the studies conducted under the "Presidents of Ukraine" grant for competitive projects (Grant No. F74/150–2017), and Grant No. F76/63–2017 of the State Fund for Fundamental Research of Ukraine.

APPENDIX: V_{eff} AND P_{ac} FOR DIFFERENT SYSTEMS

Generalized expression (7) for the maximum ac power P_{ac} that is emitted by an AFM-based SHO contains the effective frequency-dependent volume V_{eff} of a particular microwave- or terahertz-frequency system coupled to the SHO. In this appendix, we consider the method of V_{eff} calculation for the systems considered in the article. The method is based on an evaluation of the output ac power P_{ac}, which can be extracted from a SHO coupled to a particular microwave- or terahertz-frequency system, using different techniques that depend on the type of considered system, then an estimation of V_{eff} as

$$V_{\mathrm{eff}} = V\frac{P_m}{P_{\mathrm{ac}}}Q, \tag{A1}$$

where $P_m = f\mu_0 m_{\mathrm{DMI}}^2 V$ is the characteristic ac power generated in SHO by the rotating net magnetization m_{DMI}, f is the frequency of the generated signal, $V = \pi r_{\mathrm{SHO}}^2 d_{\mathrm{AFM}}$ is the volume of the AFM layer having radius r_{SHO} and thickness d_{AFM}, Q is the Q factor of the system coupled to the generating SHO, and μ_0 is the vacuum permeability. The final expressions for V_{eff} calculated in the scope of this approach for all considered microwave- or terahertz-frequency systems are presented in Table I.

1. Free space

The total power radiated in a far-field zone by a system of two almost identical magnetic dipoles can be presented as a double power radiated by one dipole. The components of the field generated by a magnetic dipole in free space (relative permittivity $\varepsilon = 1$, relative permeability $\mu = 1$) are [41]

$$\begin{aligned}
E_\phi &= -\frac{i\omega\mu_0\mathcal{M}}{4\pi}e^{-ikr}\left(\frac{ik}{r}+\frac{1}{r^2}\right)\sin\theta e^{i\omega t},\\
H_r &= \frac{i\omega\mu_0\mathcal{M}}{2\pi}e^{-ikr}\left(\frac{1}{Z_0 r^2}+\frac{1}{i\omega\mu_0 r^3}\right)\cos\theta e^{i\omega t},\\
H_\theta &= \frac{i\omega\mu_0\mathcal{M}}{4\pi}e^{-ikr}\left(\frac{i\omega\varepsilon_0}{r}+\frac{1}{Z_0 r^2}+\frac{1}{i\omega\mu_0 r^3}\right)\sin\theta e^{i\omega t},
\end{aligned} \tag{A2}$$

where $\mathcal{M} = m_{\mathrm{DMI}}V$ is the magnetic moment of the SHO's AFM layer, $\omega = 2\pi f$, $k = \omega/c$, c is the speed of light, $Z_0 = \sqrt{\mu_0/\varepsilon_0}$ is the vacuum impedance, ε_0 is the vacuum permittivity, and $i = \sqrt{-1}$. In the far-field zone, at distances $r > \lambda$ (here, λ is the wavelength of the generated signal), one can keep in Eq. (A2) only terms approximately equal to $1/r$ and can obtain a simplified form of the generated electromagnetic field:

$$\begin{aligned}
E_\phi &= \frac{\omega^2\mu_0\mathcal{M}}{4\pi c r}e^{-ikr}\sin\theta e^{i\omega t},\\
H_r &= 0,\\
H_\theta &= -\frac{\omega^2\mathcal{M}}{4\pi c^2 r}e^{-ikr}\sin\theta e^{i\omega t}.
\end{aligned}$$

The energy transfer from the dipoles into the free space is described by the time-averaged value of the Poynting vector $\mathbf{P} = \{P_r, 0, 0\}$ having only one nonzero r component:

$$P_r = \frac{1}{2}|\mathrm{Re}\{E_\phi H_\theta^*\}| = \frac{\omega^4\mu_0\mathcal{M}^2}{32c^3r^2\pi^2}\sin^2\theta.$$

The total power emitted by two magnetic dipoles can be written as

$$P_{\mathrm{ac}} = 2\oint_S \mathbf{P}d\mathbf{S} = \frac{\omega^4\mu_0\mathcal{M}^2}{6c^3\pi},$$

which, using Eq. (A1), gives, in the case $Q = 1$, an expression for the effective volume: $V_{\mathrm{eff}} = 3c^3/8\pi^3 f^3$.

2. Nanoloop

By using a nanoloop, one can extract the power generated by an AFM-based SHO in the near-field zone. In this case, the output signal in a nanoloop can be received via ac voltage induced in the loop due to the oscillations of the magnetic field (magnetic flux) inside the loop. This ac magnetic field is created by the oscillating magnetic dipoles and can be described by expressions (A2), where one should keep only terms proportional to $1/r^3$ and then neglect the others, which is the usual approach to such problems [41]. The ac voltage induced in the nanoloop by one oscillating magnetic dipole can be estimated as

$$|V_{\mathrm{dip}}| = 2\pi\mu_0\omega\left|\int_{r_{\mathrm{SHO}}}^{r_L} H(r)r dr\right| \sim \mu_0\pi f\mathcal{M}\left|\int_{r_{\mathrm{SHO}}}^{r_L}\frac{dr}{r^2}\right|,$$

where $H(r) \sim m_{\mathrm{DMI}}r_{\mathrm{SHO}}^2 d_{\mathrm{AFM}}/4r^3$ is the component of the dipole's magnetic field which is perpendicular to the loop's cross section. Taking into account that $r_{\mathrm{SHO}} \ll r_L$ and assuming that the total ac voltage induced in loop $|V_L|$ can be twice as large as $|V_{\mathrm{dip}}|$ (both voltages generated by the dipoles are in phase), the voltage $|V_L|$ can be written as $|V_L| \approx 2\pi^2\mu_0 f m_{\mathrm{DMI}}r_{\mathrm{SHO}}d_{\mathrm{AFM}}$. Then the power of extracted ac signal can be estimated as

$$P_{\mathrm{ac}} \approx \frac{|V_L|^2}{2R_L} = P_m V \frac{2\pi^2 \mu_0 f}{R_L r_{\mathrm{SHO}}^2},$$

where R_L is the resistance of the nanoloop. It follows from the written equation and Eq. (A1), where one can let $Q = 1$, that the effective volume V_{eff} is given by the expression $V_{\mathrm{eff}} = R_L r_{\mathrm{SHO}}^2 / 2\pi^2 \mu_0 f$.

3. SHO in transmission lines

In order to estimate the power of the ac signal generated in the AFM-based SHO and emitted into the transmission line, it is convenient to introduce the magnetic current density $\mathbf{j}^m = i2\pi f m_{\mathrm{DMI}}(\mathbf{x} + \mathbf{z})$, which depends on the magnetization of the AFM layer and describes the source of the electromagnetic ac field (here, $\mathbf{x}$ and $\mathbf{z}$ are the unit vectors of the x and z axes, respectively). Then, using the Lorentz lemma for electromagnetic fields in the transmission line [41], one can obtain the amplitude of the excited sth mode in the line:

$$C_s = \frac{\int_V \mathbf{j}^m \mathbf{H}_{-s} dV}{\int_{S_\perp} \{[\mathbf{E}_s \times \mathbf{H}_{-s}] - [\mathbf{E}_{-s} \times \mathbf{H}_s]\} \mathbf{z} dS}. \quad \text{(A3)}$$

Here, index s corresponds to the wave propagating in the direction $+z$, and index $-s$ corresponds to the wave propagating in the direction $-z$; $S_\perp$ is the cross-section surface of the transmission line. The ac power delivered from a SHO to the sth mode of a transmission line can be evaluated as

$$\begin{aligned} P_{\mathrm{ac},s} &= \frac{1}{2}\mathrm{Re}\left\{\int_{S_\perp} [\mathbf{E}_s \times \mathbf{H}_s^*] \mathbf{z} dS\right\} \\ &= \frac{1}{2}\mathrm{Re}\left\{\int_{S_\perp} (E_{sx} H_{sy}^* - E_{sy} H_{sx}^*) dS\right\}, \end{aligned} \quad \text{(A4)}$$

where the field components are proportional to the C_s value.

4. Rectangular waveguide

The field components of the TE_{10} mode having a unit amplitude in a hollow rectangular waveguide of cross section $a \times b$ (with a being its wide wall size and b its narrow wall size) can be written as [41]

$$\begin{aligned} H_{\pm z} &= \cos\left(\frac{\pi}{a}x\right) e^{\mp i\beta z}, \\ E_{\pm y} &= -i\omega\mu_0 \frac{a}{\pi} \sin\left(\frac{\pi}{a}x\right) e^{\mp i\beta z}, \\ H_{\pm x} &= \pm i\beta \frac{a}{\pi} \sin\left(\frac{\pi}{a}x\right) e^{\mp i\beta z}, \end{aligned}$$

where $\beta = \sqrt{(\omega^2/c^2) - (\pi^2/a^2)}$ is a propagation constant. Using these expressions for the field components of the TE_{10} mode, one can obtain from Eq. (A4)

$$P_{\mathrm{ac}} = Z_0 \frac{a^3 b}{\lambda^2} C_s^2 \sqrt{1 - \left(\frac{\lambda}{2a}\right)^2}.$$

By using the field components of the TE_{10} mode and calculating C_s from Eq. (A3), one can obtain the final expression for maximum ac power emitted from a generating SHO in the TE_{10} mode of a rectangular metal waveguide:

$$P_{\mathrm{ac}} = \frac{f^2 \mu_0 \pi^2 \mathcal{M}^2}{abc} \sqrt{1 - \left(\frac{c}{2af}\right)^2},$$

which also allows one to write the expression for V_{eff} assuming $Q = 1$: $V_{\mathrm{eff}} = 2a^2 b\chi/\pi^2$, where $\chi = \eta/\sqrt{1-\eta^2}$ and $\eta = c/2af$.

Using the same approach, one can obtain expressions for P_{ac} in any other transmission lines.

5. Dielectric waveguide

The analysis procedure for the TM_{10} mode in a dielectric waveguide, excited by the rotating net magnetization in the AFM layer of a SHO, is identical to the algorithm used for the analysis of wave excitation in a rectangular waveguide. Using the magnetic-wall boundary condition [41], one can write the field components of the TM_{10} mode in the waveguide having the cross section $a \times b$ and made of a dielectric with the relative permittivity ε:

$$\begin{aligned} E_{\pm z} &= \cos\left(\frac{\pi}{a}x\right) e^{\mp i\beta z}, \\ E_{\pm x} &= -i\beta \frac{a}{\pi} \sin\left(\frac{\pi}{a}x\right) e^{\mp i\beta z}, \\ H_{\pm y} &= \mp i\omega\varepsilon_0\varepsilon \frac{a}{\pi} \sin\left(\frac{\pi}{a}x\right) e^{\mp i\beta z}. \end{aligned}$$

Substituting these expressions into Eqs. (A3) and (A4), one can obtain the final expression for P_{ac},

$$P_{\mathrm{ac}} = \frac{\mu_0 f^2 \pi^2 \mathcal{M}^2}{abc} \sqrt{1 - \left(\frac{c}{2af\sqrt{\varepsilon}}\right)^2},$$

and can write the expression for V_{eff} assuming $Q = 1$: $V_{\mathrm{eff}} = 2a^2 b\chi_\varepsilon/\pi^2$, where $\chi_\varepsilon = \eta_\varepsilon/\sqrt{1-\eta_\varepsilon^2}$ and $\eta_\varepsilon = c/2af\sqrt{\varepsilon}$.

6. Parallel-plate line

The parallel-plate transmission line consists of two parallel metallic plates of width a, with a dielectric layer

of permittivity $\varepsilon \approx 1$ located between the plates (its thickness is b). We analyze the excitation of a fundamental T wave in the line only and assume that there is no electromagnetic field out of the line's cross section. Using Eq. (A3), the amplitude of an excited T wave can be obtained in the form

$$|C_s| = \frac{\pi f \mu_0}{2ab}\mathcal{M}.$$

The power transmitted into a parallel-plate line is given by Eq. (A4):

$$P_{\rm ac} = |C_s|^2 \frac{ab}{2Z_0} = \frac{\pi^2 {\mu_0}^2 \mathcal{M}^2 f^2}{8abZ_0},$$

which also allows one to write the expression for $V_{\rm eff}$ while assuming $Q = 1$: $V_{\rm eff} = 8abc/\pi^2 f$.

7. SHO in resonators

When an AFM-based SHO is coupled to the resonator system, one can use Maxwell's equations for the electromagnetic-field components $\mathbf{E}$ and $\mathbf{H}$, excited by a magnetic current density $\mathbf{j}^m$ [41]:

$$\mathrm{rot}\mathbf{E} + i\omega\mu_0\mu\mathbf{H} = -\mathbf{j}^m, \qquad \mathrm{rot}\mathbf{H} - i\omega\varepsilon_0\varepsilon\mathbf{E} = 0. \tag{A5}$$

The field components can be presented as a series expansion by eigenfields of the resonator [45]:

$$\mathbf{E} = \sum_n A_n \mathbf{E}_n, \qquad \mathbf{H} = \sum_n B_n \mathbf{H}_n, \tag{A6}$$

where, for simplicity, we neglect the terms dependent on gradient functions ($\mathrm{grad}\Psi_{e,h}$). The eigenfields $\mathbf{E}_n$ and $\mathbf{H}_n$ are the solutions of the uniform equations

$$\mathrm{rot}\mathbf{E}_n + i\omega_n\mu_0\mu\mathbf{H}_n = 0, \qquad \mathrm{rot}\mathbf{H}_n - i\omega_n\varepsilon_0\varepsilon\mathbf{E}_n = 0. \tag{A7}$$

They satisfy the following orthogonality conditions [45]:

$$\int_V \mathbf{E}_n^* \varepsilon_0 \varepsilon \mathbf{E}_{n'} dV = N_n^e \Delta_{nn'}, \quad \int_V \mathbf{H}_n^* \mu_0 \mu \mathbf{H}_{n'} dV = N_n^h \Delta_{nn'},$$
$$\Delta_{nn'} = \begin{cases} 1, & n = n' \\ 0, & n \neq n' \end{cases}. \tag{A8}$$

By substituting Eq. (A6) into Eq. (A5), multiplying $\mathbf{H}_n^*$ by the first obtained equation and $\mathbf{E}_n^*$ by the second one, integrating the newly obtained equations over the resonator volume V_r, and taking Eq. (A8) into account, one can get

$$\sum_n A_n \int_V \mathbf{H}_n^* \mathrm{rot}\mathbf{E}_n dV + i\omega B_n N_n^h = -\int_V \mathbf{H}_n^* \mu_0 \mu \mathbf{j}^m dV,$$
$$\sum_n B_n \int_V \mathbf{E}_n^* \mathrm{rot}\mathbf{H}_n dV - i\omega A_n N_n^e = 0. \tag{A9}$$

Using Eq. (A7), one can write Eq. (A9) in the form

$$-i\omega_n A_n N_n^h + i\omega B_n N_n^h = -i\omega G_n,$$
$$i\omega_n B_n N_n^e - i\omega A_n N_n^e = 0,$$

where $G_n = \int_V \mathbf{H}_n^* \mu_0 \mu \mathbf{m}_{\rm DMI} dV$. This system of equation has the solution

$$A_n = \frac{\omega\omega_n}{\omega_n^2 - \omega^2}\frac{G_n}{N_n^h}, \qquad B_n = \frac{\omega^2}{\omega_n^2 - \omega^2}\frac{G_n}{N_n^h}. \tag{A10}$$

To analyze the resonator excitation at the frequency $\omega \approx \omega_n$, one can introduce the Q factor of the resonator $Q_n = \omega_n/|\omega_n - \omega|$ and assume that $Q_n \gg 1$. In this case, Eq. (A10) transforms to $A_n \approx B_n \approx Q_n G_n/2N_n^h$.

The ac power pumped in the nth resonance mode by the SHO can be calculated as

$$P_{{\rm ac},n} = \frac{1}{2}(A_n^2 N_n^e + B_n^2 N_n^h). \tag{A11}$$

8. Rectangular resonator

Field components of the TE_{101} mode of a hollow rectangular resonator having the volume $a \times b \times l$ can be written in the form [41]

$$E_y = A_n \sin\left(\frac{\pi}{a}x\right)\sin\left(\frac{\pi}{l}z\right),$$
$$H_x = -i\frac{A_n}{Z_0}\frac{\lambda}{2l}\sin\left(\frac{\pi}{a}x\right)\cos\left(\frac{\pi}{l}z\right),$$
$$H_z = i\frac{A_n}{Z_0}\frac{\lambda}{2a}\cos\left(\frac{\pi}{a}x\right)\sin\left(\frac{\pi}{l}z\right).$$

The ac power pumped in the resonator by the SHO can be calculated using the maximum value of the electric field:

$$P_{\rm ac} = \frac{f}{Q}\frac{\varepsilon_0}{2}\int_0^a dx \int_0^b dy \int_0^l dz |E_{y\,\max}|^2 = \frac{\varepsilon_0 f A_n^2}{8Q}abl,$$

where $l = \lambda a/\sqrt{4a^2 - \lambda^2}$.

Assuming that the SHO can be considered a "point" object with magnetic moment $\mathcal{M}$, located in the point (x_0, y_0, z_0) inside the cavity, one can do the following estimations:

$$G_n = i\mu_0 m_{\rm DMI}\frac{1}{Z_0}\frac{\lambda}{2} \times \left[\frac{1}{l}\sin\left(\frac{\pi}{a}x_0\right)\cos\left(\frac{\pi}{l}z_0\right) - \frac{1}{a}\cos\left(\frac{\pi}{a}x_0\right)\sin\left(\frac{\pi}{l}z_0\right)\right],$$
$$N_n^h = \mu_0 abl\lambda^2(1/l^2 + 1/a^2)/16Z_0^2,$$
$$A_n \approx \frac{4Qm_{\rm DMI}Z_0 al}{b\lambda(a^2 + l^2)} \times \left[\frac{1}{l}\sin\left(\frac{\pi}{a}x_0\right)\cos\left(\frac{\pi}{l}z_0\right) - \frac{1}{a}\cos\left(\frac{\pi}{a}x_0\right)\sin\left(\frac{\pi}{l}z_0\right)\right].$$

In a typical case where $x_0 = a/2$ and $z_0 = 0$ (the SHO is attached to the center bottom of the resonator's front wall), we can obtain

$$P_{\mathrm{ac}} = 2\frac{\varepsilon_0 Q f \mathcal{M}^2 Z_0^2 a^2}{b^2\lambda^2(a^2+l^2)^2}abl,$$

which also gives $V_{\mathrm{eff}} = 8a^4 b\chi^3 f^2/c^2$.

9. Parallel-plate resonator

Here, we analyze the excitation of the T_{001} mode in a parallel-plate resonator of cross section $a \times b$ and length $l = \lambda/2$. The electromagnetic field of the T mode has the form

$$E_y = A_n \sin\left(\frac{\pi}{l}z\right), \qquad H_x = -\frac{A_n}{Z_0}\cos\left(\frac{\pi}{l}z\right).$$

Microwave power P_{ac} pumped into the resonator's mode from an AFM-based SHO can be calculated using the maximum value of the electric field:

$$P_{\mathrm{ac}} = \frac{\varepsilon_0 f}{2Q}\int_0^a dx\int_0^b dy\int_0^l dz|E_{y\max}|^2 = \frac{\varepsilon_0 f A_n^2}{4Q}abl,$$

where $A_n \approx (Q\mathcal{M}Z_0/abl)\cos[(\pi/l)z_0]$. In a typical case where $z_0 = 0$ (the SHO is attached to the front side of the resonator), one can obtain

$$P_{\mathrm{ac}} = \frac{\varepsilon_0 f Q \mathcal{M}^2 Z_0^2}{4abl}.$$

It then follows that $V_{\mathrm{eff}} = 2abc/f$.

10. Dielectric resonator

We assume that the dielectric resonator has the size $a \times b \times l$, where $l = a\lambda/\sqrt{4a^2\varepsilon - \lambda^2}$, and is made of a dielectric with permittivity ε. Using the same approach as for a rectangular resonator and magnetic-wall boundary conditions [41], one can write the field components of the TM_{101} mode:

$$E_x = \frac{iA_n}{\omega\varepsilon\varepsilon_0}\sin\left(\frac{\pi}{a}x\right)\sin\left(\frac{\pi}{l}z\right),$$
$$E_z = -\frac{iA_n}{\omega\varepsilon\varepsilon_0}\cos\left(\frac{\pi}{a}x\right)\sin\left(\frac{\pi}{l}z\right),$$
$$H_y = A_n\sin\left(\frac{\pi}{a}x\right)\sin\left(\frac{\pi}{l}z\right).$$

Then the ac power pumped in the resonator from the SHO can be evaluated as

$$P_{\mathrm{ac}} = \frac{f}{Q}\frac{\mu_0}{2}\int_0^a dx\int_0^b dy\int_0^l dz|H_{y\max}|^2 = \frac{\mu_0 f A_n^2}{8Q}abl.$$

Assuming that the SHO can be considered a point object with magnetic moment $\mathcal{M}$, located in the point (x_0, y_0, z_0), we obtain $A_n \approx (2Q\mathcal{M}/abl)\sin[(\pi/a)x_0]\sin[(\pi/l)z_0]$. In a typical case where $x_0 = a/2$ and $z_0 = 0$ (the SHO is attached to the center bottom of the resonator's front wall), an expression for the output power transforms to its final form:

$$P_{\mathrm{ac}} = \frac{\mu_0 f Q \mathcal{M}^2}{2abl}.$$

Thus, $V_{\mathrm{eff}} = 2a^2 b\chi_\varepsilon$, where $\chi_\varepsilon = \eta_\varepsilon/\sqrt{1-\eta_\varepsilon^2}$ and $\eta_\varepsilon = c/2af\sqrt{\varepsilon}$.

[1] C. Sirtori, Applied physics: Bridge for the terahertz gap, Nature (London) **417**, 132 (2002).

[2] R. Kleiner, Filling the terahertz gap, Science **318**, 1254 (2007).

[3] Yu. V. Gulyaev, P. E. Zilberman, G. M. Mikhailov, and S. G. Chigarev, Generation of terahertz waves by a current in magnetic junctions, JETP Lett. **98**, 742 (2014).

[4] E. A. Nanni, W. R. Huang, K.-H. Hong, K. Ravi, A. Fallahi, G. Moriena, R. J. D. Miller, and F. X. Kärtner, Terahertz-driven linear electron acceleration, Nat. Commun. **6**, 8486 (2015).

[5] M. V. Kartikeyan, E. Borie, and M. Thumm, *Gyrotrons: High Power Microwave and Millimeter Wave Technology* (Springer, New York, 2004).

[6] H.-W. Hübers, Terahertz technology: Towards THz integrated photonics, Nat. Photonics **4**, 503 (2010).

[7] L. Consolino, S. Jung, A. Campa, M. De Regis, S. Pal, J. H. Kim, K. Fujita, A. Ito, M. Hitaka, S. Bartalini, P. De Natale, M. A. Belkin, and M. S. Vitiello, Spectral purity and tunability of terahertz quantum cascade laser sources based on intracavity difference-frequency generation, Sci. Adv. **3**, e1603317 (2017).

[8] L. Ozyuzer, A. E. Koshelev, C. Kurter, N. Gopalsami, Q. Li, M. Tachiki, K. Kadowaki, T. Yamamoto, H. Minami, H. Yamaguchi, T. Tachiki, K. E. Gray, W.-K. Kwok, and U. Welp, Emission of coherent THz radiation from superconductors, Science **318**, 1291 (2007).

[9] B. Gorshunov, A. Volkov, I. Spektor, A. Prokhorov, A. Mukhin, M. Dressel, S. Uchida, and A. Loidl, Terahertz BWO-spectrosopy, Int. J. Infrared Millim. Waves **26**, 1217 (2005).

[10] M. Tonouchi, Cutting-edge terahertz technology, Nat. Photonics **1**, 97 (2007).

[11] T. Chen, R. K. Dumas, A. Eklund, P. K. Muduli, A. Houshang, A. A. Awad, P. Dürrenfeld, B. G. Malm, A. Rusu, and J. Åkerman, Spin-torque and spin-Hall nano-oscillators, Proc. IEEE **104**, 1919 (2016).

[12] M. Tsoi, A. G. M. Jansen, J. Bass, W.-C. Chiang, V. Tsoi, and P. Wyder, Generation and detection of phase-coherent

current-driven magnons in magnetic multilayers, Nature (London) **406**, 46 (2000).
[13] S. I. Kiselev, J. C. Sankey, I. N. Krivorotov, N. C. Emley, R. J. Schoelkopf, R. A. Buhrman, and D. C. Ralph, Microwave oscillations of a nanomagnet driven by a spin-polarized current, Nature (London) **425**, 380 (2003).
[14] W. H. Rippard, M. R. Pufall, S. Kaka, S. E. Russek, and T. J. Silva, Direct-Current Induced Dynamics in $Co_{90}Fe_{10}$/$Ni_{80}Fe_{20}$ Point Contacts, Phys. Rev. Lett. **92**, 027201 (2004).
[15] V. E. Demidov, S. Urazhdin, H. Ulrichs, V. Tiberkevich, A. Slavin, D. Baither, G. Schmitz, and S. O. Demokritov, Magnetic nano-oscillator driven by pure spin-current, Nat. Mater. **11**, 1028 (2012).
[16] S. M. Mohseni, S. R. Sani, J. Persson, T. N. Anh Nguyen, S. Chung, Ye. Pogoryelov, P. K. Muduli, E. Iacocca, A. Eklund, R. K. Dumas, S. Bonetti, A. Deac, M. A. Hoefer, and J. Åkerman, Spin torque-generated magnetic droplet solitons, Science **339**, 1295 (2013).
[17] J. D. Costa, S. Serrano-Guisan, B. Lacoste, A. S. Jenkins, T. Böhnert, M. Tarequzzaman, J. Borme, F. L. Deepak, E. Paz, J. Ventura, R. Ferreira, and P. P. Freitas, High power and low critical current density spin transfer torque nano-oscillators using MgO barriers with intermediate thickness, Sci. Rep. **7**, 7237 (2017).
[18] S. Bonetti, P. Muduli, F. Mancoff, and Johan Åkerman, Spin torque oscillator frequency versus magnetic field angle: The prospect of operation beyond 65 GHz, Appl. Phys. Lett. **94**, 102507 (2009).
[19] H. V. Gomonay and V. M. Loktev, Spin transfer and current-induced switching in antiferromagnets, Phys. Rev. B **81**, 144427 (2010).
[20] E. V. Gomonay and V. M. Loktev, Spintronics of antiferromagnetic systems, Low Temp. Phys. **40**, 17 (2014).
[21] R. Cheng, D. Xiao, and A. Brataas, Terahertz Antiferromagnetic Spin Hall Nano-oscillator, Phys. Rev. Lett. **116**, 207603 (2016).
[22] R. Khymyn, I. Lisenkov, V. Tiberkevich, B. A. Ivanov, and A. Slavin, Antiferromagnetic THz-frequency Josephson-like oscillator driven by spin current, Sci. Rep. **7**, 43705 (2017).
[23] P. Wadley *et al.*, Electrical switching of an antiferromagnet, Science **351**, 587 (2016).
[24] D. Kriegner, K. Výborný, K. Olejník, H. Reichlová, V. Novák, X. Marti, J. Gazquez, V. Saidl, P. Němec, V. V. Volobuev, G. Springholz, V. Holý, and T. Jungwirth, Multiple-stable anisotropic magnetoresistance memory in antiferromagnetic MnTe, Nat. Commun. **7**, 11623 (2016).
[25] T. Jungwirth, J. Wunderlich, and K. Olejník, Spin Hall effect devices, Nat. Mater. **11**, 382 (2012).
[26] V. E. Demidov, S. Urazhdin, A. Zholud, A. V. Sadovnikov, and S. O. Demokritov, Nanoconstriction-based spin-Hall nano-oscillator, Appl. Phys. Lett. **105**, 172410 (2014).
[27] L. Berger, Emission of spin waves by a magnetic multilayer traversed by a current, Phys. Rev. B **54**, 9353 (1996).
[28] J. C. Slonczewski, Current-driven excitation of magnetic multilayers, J. Magn. Magn. Mater. **159**, L1 (1996).
[29] H. Nakayama, K. Ando, K. Harii, T. Yoshino, R. Takahashi, Y. Kajiwara, K. Uchida, Y. Fujikawa, and E. Saitoh, Geometry dependence on inverse spin Hall effect induced by spin pumping in $Ni_{81}Fe_{19}$/Pt films, Phys. Rev. B **85**, 144408 (2012).
[30] P. W. Anderson, F. R. Merrit, J. P. Remeika, and W. A. Yager, Magnetic resonance in α-Fe_2O_3, Phys. Rev. **93**, 717 (1954).
[31] A. H. Morrish, *Canted Antiferromagnetism: Hematite* (World Scientific, Singapore, 1995).
[32] E. A. Turov, A. V. Kolchanov, M. I. Kurkin, I. F. Mirsaev, and V. V. Nikolaev, *Symmetry and Physical Properties of Antiferromagnets* (Cambridge International Science Publishing, Cambridge, England, 2010).
[33] H. Kumagai, H. Abe, and K.Ôno, I. Hayashi, J. Shimada, and K. Iwanaga, Frequency dependence of magnetic resonance in α-Fe_2O_3, Phys. Rev. **99**, 1116 (1955).
[34] G. Rollmann, A. Rohrbach, P. Entel, and J. Hafner, First-principles calculation of the structure and magnetic phases of hematite, Phys. Rev. B **69**, 165107 (2004).
[35] M. N. Huda, A. Walsh, Y. Yan, S.-H. Wei, and M. M. Al-Jassim, Electronic, structural, and magnetic effects of 3*d* transition metals in hematite, J. Appl. Phys. **107**, 123712 (2010).
[36] M. Catti, G. Valerio, and R. Dovesi, Theoretical study of electronic, magnetic, and structural properties of α-Fe_2O_3 (hematite), Phys. Rev. B **51**, 7441 (1995).
[37] R. Cheng, J. Xiao, Q. Niu, and A. Brataas, Spin Pumping and Spin-Transfer Torques in Antiferromagnets, Phys. Rev. Lett. **113**, 057601 (2014).
[38] J. Xiao, G. E. W. Bauer, K. Uchida, E. Saitoh, and S. Maekawa, Theory of magnon-driven spin Seebeck effect, Phys. Rev. B **81**, 214418 (2010).
[39] O. Prokopenko, E. Bankowski, T. Meitzler, V. Tiberkevich, and A. Slavin, Spin-torque nano-oscillator as a microwave signal source, IEEE Magn. Lett. **2**, 3000104 (2011).
[40] N. Amin, H. Xi, and M. X. Tang, Analysis of electromagnetic fields generated by a spin-torque oscillator, IEEE Trans. Magn. **45**, 4183 (2009).
[41] S. Ramo, J. R. Whinnery, and T. Van Duzer, *Fields and Waves in Communication Electronics* (John Wiley & Sons, New York, 1984).
[42] We choose the following qualitative approximations for the frequency-dependent Q factor: $Q(f) = Q_0(f_0/f)^{3/2}$ for the rectangular resonator ($Q_0 = 10^5$ at $f_0 = 1$ GHz), $Q(f) = Q_0(f_0/f)$ for the parallel-plate resonator ($Q_0 = 10^3$ at $f_0 = 1$ GHz), and $Q(f) = Q_0(f_0/f)^{1/3}$ for the dielectric resonator ($Q_0 = 6 \times 10^3$ at $f_0 = 1$ GHz).
[43] R. Köhler, A. Tredicucci, F. Beltram, H. E. Beere, E. H. Linfield, A. G. Davies, D. A. Ritchie, R. C. Iotti, and F. Rossi, Terahertz semiconductor-heterostructure laser, Nature (London) **417**, 156 (2002).
[44] R. H. Liu, W. L. Lim, and S. Urazhdin, Spectral Characteristics of the Microwave Emission by the Spin Hall Nano-oscillator, Phys. Rev. Lett. **110**, 147601 (2013).
[45] A. G. Gurevich and G. A. Melkov, *Magnetization Oscillations and Waves* (CRC Press, Boca Raton, 1996).